Experiments in Fluids 32 (2002) 229–241 © Springer-Verlag 2002
DOI 10.1007/s003480100353

Experimental study of boundary-layer transition on an airfoil induced by periodically passing wake

W.-P. Jeon, T.-C. Park, S.-H. Kang

Abstract Hot-wire measurements are performed in boundary-layer flows developing on a NACA 0012 airfoil over which wakes pass periodically. The periodic wakes are generated by rotating circular cylinders clockwise or counterclockwise around the airfoil. The time- and phase-averaged mean streamwise velocities and turbulence fluctuations are measured to investigate the phenomena of wake-induced transition. Especially, the phase-averaged wall shear stresses are evaluated using a computational Preston tube method. The passing wakes significantly change the pressure distribution on the airfoil, which has influence on the transition process of the boundary layer. The orientation of the passing wake alters the pressure distribution in a different manner. Due to the passing wake, the turbulent patches are generated inside the laminar boundary layer on the airfoil, and the boundary layer becomes temporarily transitional. The patches propagate downstream at a speed smaller than the free-stream velocity and merge together further downstream. Relatively high values of phase-averaged turbulence fluctuations in the outer part of the boundary layer indicate the possibility that breakdown occurs in the outer layer away from the wall. It is confirmed that the phase-averaged mean velocity profile has two dips in the outer region of the transitional boundary layer for each passing cycle.

1 Introduction

Unsteady boundary-layer flows over the blades in turbomachinery have received attention since they strongly affect fluid-dynamic performance, flow loss and heat transfer on the blades. In a multi-stage axial compressor and turbine, periodic passing-wakes from an upstream blade impose a considerable influence on boundary-layer development and especially on the transition process over the downstream blade surface, in which it is known that wake-induced transition occurs. Therefore, correct understanding and accurate prediction of the wake-induced transitional flow are important to design a highly efficient blade.

A number of experiments on wake-induced transition in turbomachinery were reported by Dong and Cumpsty (1990a, b), Mayle and Dullenkopf (1991), Halstead et al. (1997), Schulte and Hodson (1998), and Walker et al. (1999) (see also the reviews by Mayle (1991) and Walker (1993)). Although these compressor and turbine experiments provided important aspects of unsteady boundary-layer flows in practical environments, various unsteady disturbances in complex turbomachine flows made it difficult to investigate the effect of the passing wakes on the boundary-layer development. Complex geometries of conventional turbomachines also made it difficult to obtain high quality data near the blade surface. To overcome such technical limitations, a number of investigators have performed hot-wire measurements for wake-induced transition on a flat plate in a wind tunnel (Pfeil et al. 1983; Liu and Rodi 1991; Orth 1993; Funazaki and Koyabu 1999; Funazaki and Aoyama 2000). In their experiments, the periodic unsteady blade-row disturbances were simplified as periodic passing-cylinder wakes, which were generated upstream of the plate by a rotating squirrel wheel. Liu and Rodi (1991) measured time- and phase-averaged mean and fluctuating streamwise velocity profiles in wake-affected boundary layers for four different wake-passing frequencies. Funazaki and Koyabu (1999) focused on the effects of periodic passing wakes on boundary-layer transition on a flat plate under the favorable and adverse pressure gradients. With the same facilities and experimental conditions, Funazaki and Aoyama (2000) measured two component velocities using a split-film probe. On the other hand, numerical simulations were also carried out to predict flow and heat-transfer characteristics in wake-affected transitional boundary layers (Cho et al. 1993; Fan and Lakshminarayana 1996; Chakka and Schobeiri 1999; Kim and Crawford 2000). Very recently, Wu et al. (1999) conducted a three-dimensional, time-accurate direct numerical simulation of wake-induced boundary-layer transition. They reported detailed behavior such as generation, growth, and

Received: 12 February 2001 / Accepted: 6 July 2001
Published online: 23 November 2001

W.-P. Jeon (✉)
Center for Turbulence and Flow Control Research
Institute of Advanced Machinery and Design
Seoul National University, Seoul 151-742, Korea
e-mail: wpjeon@plaza1.snu.ac.kr

T.-C. Park, S.-H. Kang
School of Mechanical and Aerospace Engineering
Seoul National University, Seoul 151-742, Korea

The present work was supported by the Korea Ministry of Education (96ME-B-04) and National Creative Research Initiatives of the Korean Ministry of Science and Technology. The authors wish to thank Professor Haecheon Choi for helpful discussions.

coalescence of wake-induced turbulent patches in the boundary-layer flows, and provided many useful time- and phase-averaged flow data.

As mentioned in previous work, the wake-affected boundary-layer transition strongly depends upon the characteristics of wake-induced turbulent patches. When wakes pass over a laminar boundary-layer flow, turbulent patches are generated inside the boundary layers and the flow becomes temporarily transitional. When going downstream, the patches grow and merge with each other due to different propagation speeds of their leading and trailing edges. When the patches coalesce sufficiently at the far downstream station, the boundary-layer flow becomes fully turbulent. Initial turbulent patches at the leading edge of the test plate are mainly subjected to turbulence intensities and mean velocity defects of passing wakes. On the other hand, their growth is affected by various internal and external flow conditions such as the characteristics of the initial turbulent patch and traveling wake, the streamwise pressure distribution, the free-stream turbulence intensity. Hence, understanding the behavior of the turbulent patch under certain external flow fields is required to predict the wake-induced transitional boundary-layer flows.

This work is a fundamental study of wake-induced transition employing a NACA 0012 airfoil with zero angle of attack instead of a real turbomachine blade. The passing wakes are generated by rotating circular cylinders clockwise (CW) or counterclockwise (CCW) around the airfoil, so the wake passes consecutively over the airfoil at each passing period. The time- and phase-averaged streamwise mean velocities and turbulence fluctuations in the boundary-layer flows are precisely measured using a single hot-wire probe. The phase-averaged wall shear stresses are evaluated using a computational Preston tube method (Nitsche et al. 1983). From the measured data, we investigate the characteristics of the wake-affected turbulent patch in connection to the phenomena of wake-induced transition.

2
Experimental set-up and method

2.1
Apparatus and instrumentation

The experiments were conducted in a closed-type wind tunnel. The test section was a rectangle of 0.6 m wide, 0.3 m high, and 2.0 m long. At the free-stream speed of 10 m/s, the uniformity of the streamwise mean velocity and turbulence intensity at the test section was less than 0.4 and 0.5%, respectively. The zero streamwise static pressure gradient in the test section without the airfoil was obtained by adjusting the side walls.

Figure 1a shows a schematic of the airfoil, the wake-generating wheel and the traverse unit for the hot-wire probe in the test section. A rotating disk of the wheel was at the bottom wall of the test section and was driven by a continuously adjustable DC motor at the exterior of the wind tunnel. Eight circular cylinders of 3 mm diameter were vertically installed and equally spaced along the circumference of the rotating disk. The cylinders in the wheel moved along the circular path with a radius of 0.27 m perpendicular to the incoming flow in front of the airfoil, so the periodic two-dimensional passing wakes were generated and affected the flow over the downstream airfoil. As shown in Fig. 1b, the cylinders rotated CW or CCW (when seeing the wheel over the test section) around the airfoil at the same speed to the incoming flow velocity of 10 m/s. Therefore, the wake-generating frequency was 47.2 Hz and the Strouhal number based on airfoil chord length ($St_C = fC/U_\infty$) was 1.416. When the cylinder was positioned just in front of the airfoil, the distance between the center of the cylinder and airfoil leading edge was 0.12 m. The test blade made of an aluminum alloy was a NACA 0012 airfoil and its chord length and width were 0.3 and 0.29 m, respectively. The Reynolds number based on the chord length and the incoming free-stream velocity was 2×10^5. Forty holes of 0.8 mm diameter were made on the airfoil to measure static pressure. The airfoil was vertically mounted with zero angle of attack at the center of the test section and detached from the rotating disk with a gap of 5 mm. The height of the near-wall flow disturbed by the rotating disk was found to be less than 10% of airfoil width at 10 m/s. Therefore, this disturbance did not affect the wake-induced boundary-layer flows over the mid-span of the airfoil in real experiments.

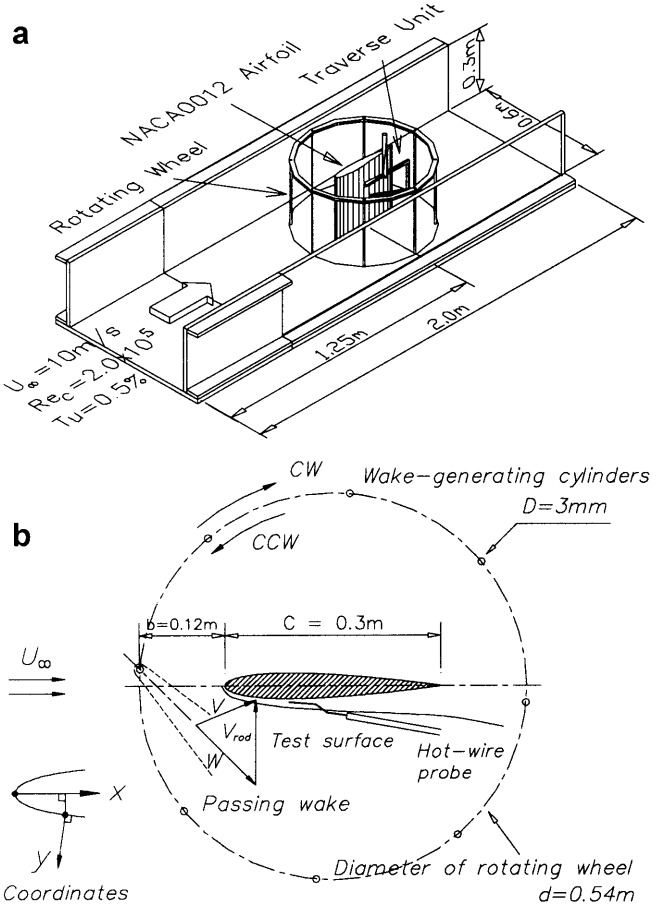

Fig. 1a, b. Schematic of the test equipment: **a** a 3-D view, **b** an overview

A single hot-wire probe was positioned in the flow by a traverse (0.01 mm resolution) placed on the roof of the test section and controlled automatically by a computer via a stepping motor. The specially designed disk, which was mounted on the upper wall of the test section, enabled the probe to move perpendicularly to each streamwise location of the airfoil.

Instantaneous streamwise velocities were measured in the boundary layers with a single hot-wire probe (Dantec 55P15). To obtain phase information of the flow fields, the hot-wire signal was synchronized with wake-passing time using a photocell installed on the rotating disk. The signals from the hot-wire anemometer and the photocell were all recorded via 12-bit analog-to-digital converter (Data Translation 2833) by the computer. At each x location, the output from the hot-wire anemometer was sampled at a rate of 8.75 kHz for 56 s.

The maximum deviation of calibrated velocity is 1.0% when compared with the recalibrated velocity after the measurement. Considering other uncertainty factors in the hot-wire measurement, the uncertainty level of the measured velocity is less than 2%.

2.2
Analysis of velocity component

The instantaneous streamwise velocity in the periodic unsteady flow is expressed in the form of

$$u = \langle U \rangle + u' = \bar{U} + \tilde{u} + u' \tag{1}$$

where $\langle U \rangle$ is the phase-averaged velocity, which is composed of the time-averaged velocity $\bar{U}$ and the periodic velocity fluctuation $\tilde{u}$, and u' is the stochastic turbulence fluctuation. The phase-averaged rms value of the turbulence fluctuation is determined from

$$\sqrt{\langle u'^2 \rangle} = \sqrt{\frac{1}{N}\sum_{i=1}^{N} (u_i - \langle U \rangle)^2} \tag{2}$$

where N is the sampled number of velocity traces for ensemble-averaging process. At each measuring point, the 490,000 velocity data were obtained during the wake passes over 2,600 times, which corresponds to $N = 330$.

2.3
Estimation of wall skin friction

The local wall skin friction is an important and sensitive parameter showing the characteristics of transitional boundary layers. In the present study, a computational Preston tube method (CPM), proposed by Nitsche et al. (1983), was used to estimate the local wall skin friction. Jeon and Kang (1995) demonstrated that the CPM was useful for predicting wall skin frictions in transitional boundary layers on a flat plate. Very recently, using previous DNS and experimental databases, Jeon et al. (2000) showed that wall skin friction in transition regions could be estimated via the CPM with good accuracy regardless of free-stream conditions (e.g., turbulence intensity, streamwise pressure gradient). Also, Lee and Kang (2000) reasonably obtained wall skin frictions in transitional boundary layers on an airfoil subjected to a steady turbulent wake.

In the present study, the phase-averaged wall skin frictions are obtained using the measured phase-averaged near-wall velocities via the CPM. These data are very useful for understanding the behavior of wake-induced turbulent patches and the unsteady transition process.

3
Results and discussion

3.1
Base flow

Figure 2 shows streamwise distributions of the time-averaged pressure on the test surface of the airfoil without and with the passing wakes. The pressure profiles in the presence of passing wakes are discussed at Sect. 3.2.1 of this paper. Without the passing wakes, the static pressure distributions on the test and its opposite surface are in good agreement with each other, indicating that the airfoil is mounted with zero angle of attack at the center of the test section and two-dimensional boundary layers develop along the mid-span of the airfoil. The measured pressure profile shifts down from an inviscid solution of the NACA 0012 airfoil in the infinite flow. This is due to the blockage effect of the sidewall of the test section. However, the measured profile agrees quite well with another inviscid solution where the blockage effect is taken into account. The large favorable pressure gradient exists near the leading edge followed by the adverse pressure gradient from $x/C = 0.15$ to the trailing edge.

The measured time-averaged velocities (not shown here) exhibit laminar boundary-layer profiles dependent on the local pressure gradients. The velocities subjected to the favorable pressure gradients near the leading edge are larger than Blasius solution in most y positions, however, the flow is affected by the adverse pressure gradients at the downstream stations. Turbulence intensity profile (not shown here) at each x station has a peak near the wall. The peak has the value of about 1% at $x/C = 0.1$ and increases very slowly along the downstream station, but at the last measuring station ($x/C = 0.85$), it jumps up suddenly to a value of about 5%. This means that instability starts from

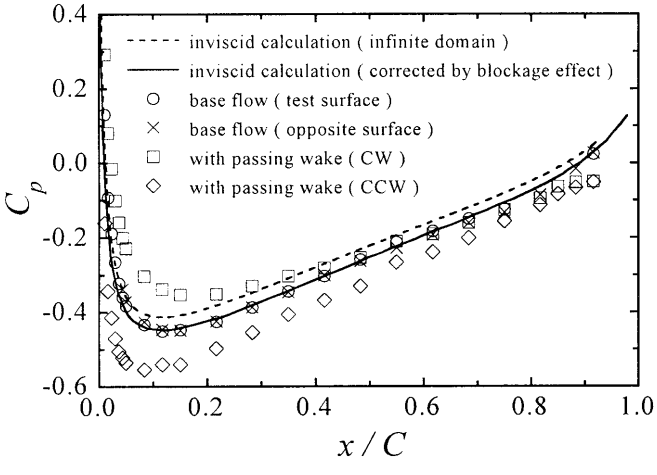

Fig. 2. Static pressure coefficients on the airfoil without and with passing wakes

at least $x/C = 0.85$ although the measured mean velocities still show the laminar profile at this station.

3.2
Unsteady flow disturbed by passing wakes

3.2.1
Time-averaged pressure on the airfoil

The streamwise profile of time-averaged pressure on the airfoil is greatly changed by the passing wakes as shown in Fig. 2. It can be also seen that the passing-wake orientation has different effects on the pressure distributions. In the case of CW rotation, the pressure is larger than that without passing wake up $x/C = 0.5$ and then slightly smaller at $x/C > 0.7$. The minimum pressure coefficient increases by 20% and its x location moves slightly downstream, i.e., from $x/C = 0.11$ to 0.15. Consequently, the passing wakes for the CW case alleviate the pressure gradients on the airfoil: the favorable pressure gradient region near the leading edge becomes broader, and the adverse pressure gradient downstream of $x/C = 0.15$ is reduced. On the other hand, in the case of CCW rotation, the pressure decreases on the whole x stations as compared to the case without passing wake. The minimum pressure coefficient decreases by 30% and its x location moves slightly upstream (to $x/C = 0.08$). This indicates that for the CCW case, the favorable pressure gradient region becomes narrow and the adverse pressure gradient increases downstream of $x/C = 0.08$.

Hodson (1985) explained this change of the pressure profile due to the passing wakes as a concept of "negative jet". Figure 1b shows a temporal velocity triangle near the leading edge of the test surface for the CW case. When the cylinder moves up with V_{rod}, a velocity inside the wake is denoted as W in the relative frame. As a result, in the stationary frame, the inlet flow has a resultant velocity V. The vertical velocity component of V causes a high-pressure stagnation point near the leading edge and consequently, alleviates the pressure gradient on the airfoil. Hodson (1985) thought that this effect resulted from a vertical component of the negative relative wake-velocity, i.e., $-W$ (negative jet). When V_{rod} moves down (CCW case), the vertical velocity component of V results in reducing static pressure near the leading edge, so the adverse pressure gradient becomes larger, as shown in Fig. 2. Wu et al. (1999) from a direct numerical simulation checked the effect of the wake orientation on the streamwise pressure distribution and reported similar results to those of the current study.

3.2.2
Characteristics of a turbulent patch

Figure 3a, b present iso-surfaces of the phase-averaged turbulence intensity of 8% in an x–y–t domain for the cases of CW and CCW, respectively, where T denotes the wake-passing period (21.2 ms). The turbulent patch is periodically generated near the leading edge due to passing wake. The patches grow gradually in the x and y directions as they move downstream and merge together further downstream. After merging, they grow more rapidly in the y direction.

The turbulent patch near the leading edge for the CCW case is larger and convects more quickly than that for the CW case. In addition, the patches for the CCW case grow faster in the x and y directions, and merge earlier than for the CW case. This fact implies that in the time-averaged sense, transition onset for the CCW case arises further upstream in comparison with that for the CW case. The larger and stronger upstream turbulent patch for the CCW case is attributed to the relatively higher turbulence intensity inside the passing wake that impacts on the test surface near the leading edge and then interacts with the initial laminar boundary layer. The faster growth and earlier merging of the patches for the CCW case seem to result not only from the higher turbulence intensity inside the upstream patch but also from larger streamwise adverse pressure gradient (see Fig. 2). Funazaki and Koyabu (1999) reported that turbulent patches expanded more quickly in the streamwise and wall-normal directions under the adverse pressure gradient than the favorable pressure gradient. Gostelow et al. (1996) also revealed that the propagation of the turbulent patch becomes faster with larger adverse pressure gradient. Thus, the present result that the growth rate of the turbulent patch for the CCW

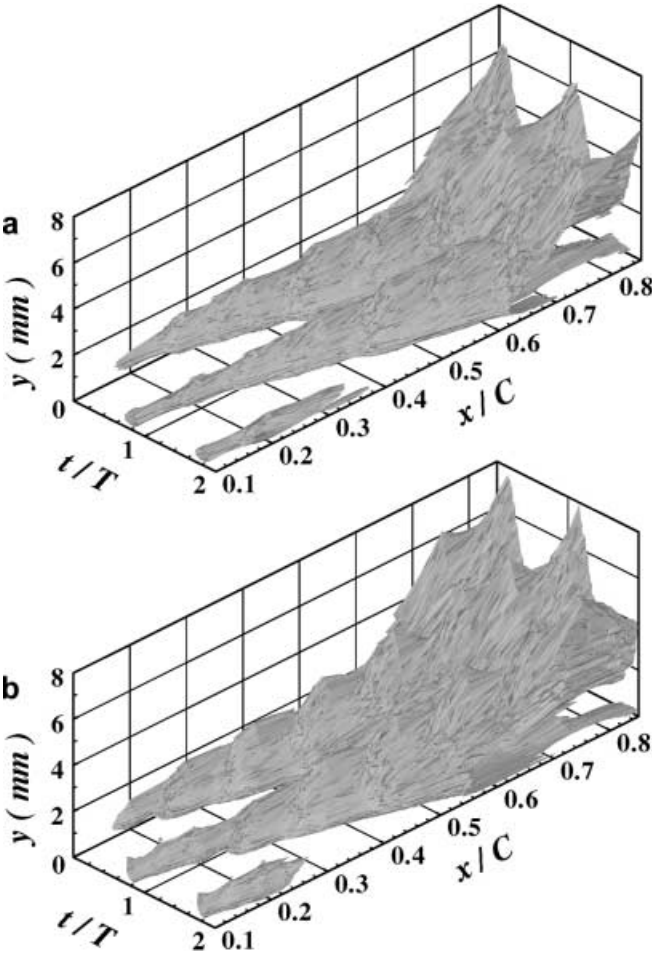

Fig. 3a, b. Iso-surface contour of the turbulence intensity, $\sqrt{\langle u'^2 \rangle}/U_\infty = 8\%$ in the cases of **a** CW rotation and **b** CCW rotation

case is higher than that for the CW case, is one evidence to support those previous results.

To investigate behaviors of the turbulent patch in more detail, contours of the phase-averaged turbulence intensity are plotted in an x–y plane as shown in Fig. 4a, b. This figure represents six sequential snapshots during one wake-passing period T for the cases of CW and CCW. The $t/T = 0$ is the moment when the rotating cylinder aligns with the leading edge of the airfoil. The passing wakes at the map of each instant are identified as columns of contour lines that are highly extended along the y direction. At $t/T = 4/6$, the wake appears near the leading edge for both CW and CCW cases and moves downstream at the free-stream velocity. It is also seen that the wake-induced turbulent patch appears beneath the traveling wake. As the wake convects downward (see the map at $t/T = 5/6$ and 0), the leading edge of the turbulent patch moves almost at the same speed of the wake, while the trailing edge propagates at less speed than the wake-convecting speed. This causes the patches to gradually expand in the streamwise direction and finally start merging with each other at a downstream station (see the map at $t/T = 1/6$). The features of the turbulent patches observed in this study are very similar to other experimental results (Pfeil et al. 1983; Liu and Rodi 1991; Funazaki and Koyabu 1999).

It is also seen from these maps that the wake-induced patch for the CCW case lags further behind the preceding wake than that for the CW case, and it finally separates from the wake after $t/T = 3/6$. This means that the turbulent patch for the CCW case grows more rapidly in the streamwise direction than that for the CW case. The separation between the wake and the turbulent patch in

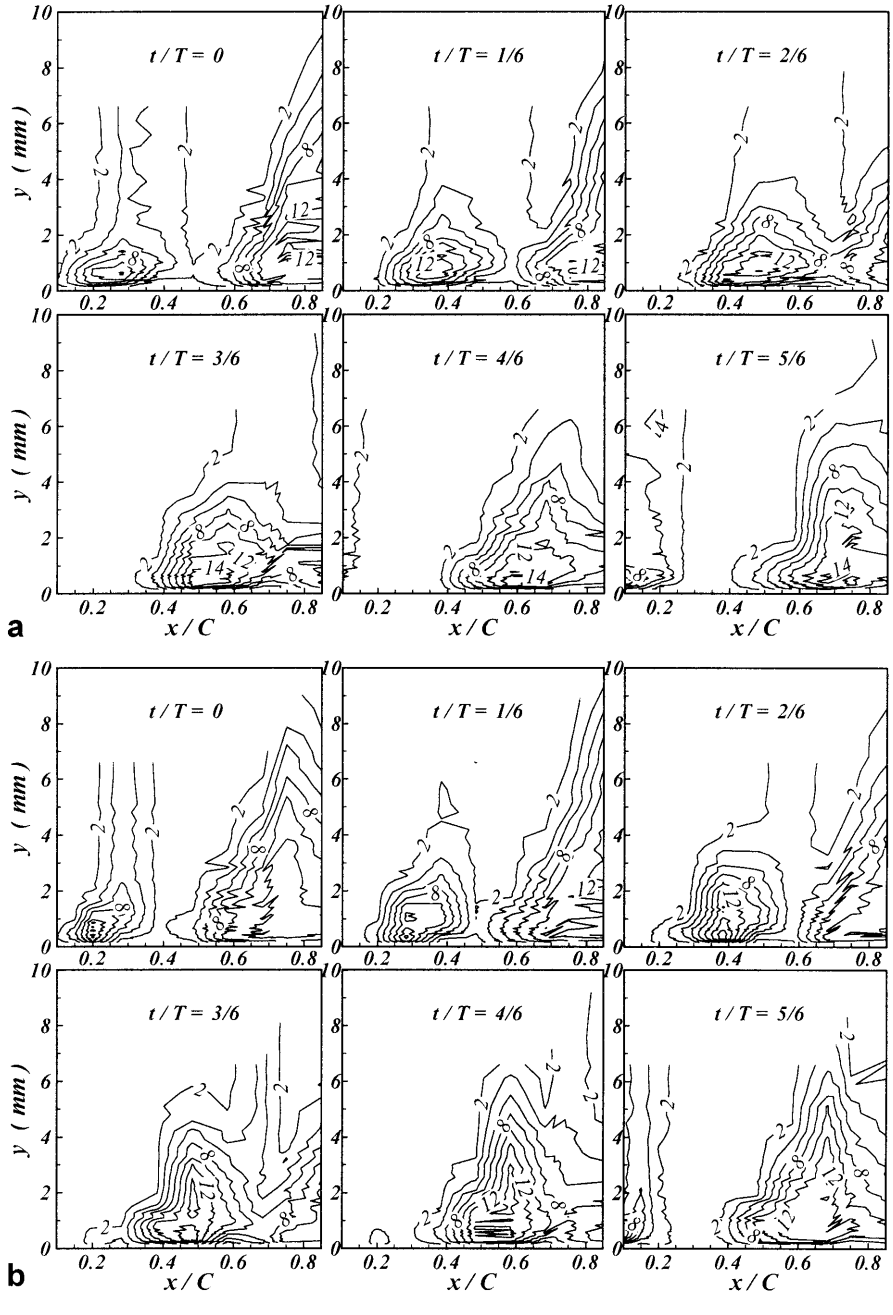

Fig. 4a, b. Contours of the phase-averaged turbulence intensity (%) in an x–y plane for **a** the CW case and **b** the CCW case

wake-affected boundary-layer flows was also reported by Orth (1993). Funazaki and Aoyama (2000) also found this separation only for the "the reverse rotation case", i.e., when the wake-generating cylinder moved away from the test surface, which is consistent with our result for the CCW case.

Figure 5 presents contours of the phase-averaged turbulence intensity in the x–t plane at $y = 0.66$ mm for the CCW case. As shown in Fig. 4b, around this y position the turbulent patches expand most rapidly in the streamwise direction for the CCW case. The leading edge of the turbulent patch propagates almost at the speed of the incoming flow U_∞, whereas the trailing edge convects with a speed smaller than U_∞. In addition, due to the streamwise adverse pressure gradient, the trailing edge of the turbulent patch is found to propagate more and more slowly along the downstream station.

To estimate the magnitude of the local leading or trailing edge propagation speed, a reasonable threshold value of a certain flow quantity for the identification of the turbulent patch must be chosen. Gostelow et al. (1996) selected the value of 2% mean velocity perturbation and 4% turbulence intensity as the threshold values for the determination of the leading and trailing edge of the patch, respectively. In Fig. 5, the contour lines around the turbulent patch are found to be almost parallel for the four different levels of the turbulence intensity such as 4, 6, 8, and 10%, indicating that the leading and trailing edge velocities are not sensitive to the threshold value selected. Therefore, in the present study, a turbulence intensity level of 4% is regarded as a representative threshold value for the determination of the leading and trailing edge of the patch. Based on this threshold value, the local leading- and trailing-edge convection velocities at $y = 0.66$ mm for the CCW case are $0.81 \sim 0.86\ U_\infty$ and $0.38 \sim 0.41\ U_\infty$, respectively. The corresponding velocities at the same y position for the CW case (x–t map is not shown here) are $0.87 \sim 0.91\ U_\infty$ and $0.43 \sim 0.50\ U_\infty$, respectively. The turbulent patches are found to merge with each other around $x/C = 0.6$ and 0.5 for the CW and CCW cases, respectively.

3.2.3 Time-averaged boundary-layer properties

Figure 6 shows time-averaged wall skin frictions which are estimated using the CPM. The characteristic velocity on Re_x and $\overline{C_f}$ is the boundary-layer edge velocity $\overline{U_e}$. For the base flow, $\overline{C_f}$ decreases monotonously along the downstream station and its profile shows a typical laminar distribution subjected to streamwise adverse pressure gradients. $\overline{C_f}$ at $x/C = 0.1$ ($Re_x = 24{,}800$) is slightly larger than the Blasius solution due to the local favorable pressure gradient. However, downstream of $x/C = 0.2$, it becomes lower than Blasius solution due to the adverse pressure gradient. $\overline{C_f}$ for the base flow can also be estimated from linear fitting of near-wall velocities with the relation of $\overline{C_f} = \left(2\nu/\overline{U_e}^2\right)\left(\mathrm{d}\overline{U}/\mathrm{d}y\right)$ because all boundary layers over the airfoil are laminar. $\overline{C_f}$ from the linear fitting method is found to agree well with that from the CPM. With the passing wakes, the occurrence of transition can be identified from the abrupt rise in $\overline{C_f}$. If the position of transition onset is defined as the streamwise location of a minimum skin friction, it can be seen that transition for the CCW case (onset point: $x/C = 0.38$) starts earlier than for the CW case (onset point: $x/C = 0.48$). For both CW and CCW cases, transition is not completed even at the last measuring streamwise location. For the CCW case, upstream of transition-onset point, i.e., in the laminar regions, $\overline{C_f}$ is lower than that of the base flow as well as Blasius solution because the streamwise adverse pressure gradient is larger as explained in Sect. 3.2.1.

Time-averaged mean streamwise velocities at six x locations for the CCW case are plotted in wall coordinates as shown in Fig. 7. Time-averaged mean friction velocities $\overline{u_\tau}$ used for the calculation of wall variables, y^+, $\overline{U}^+$ are obtained from the CPM. Before transition starts, the mean velocity distribution over the airfoil shows a typical laminar profile although the turbulent patch passes periodically through the boundary layer. As moving

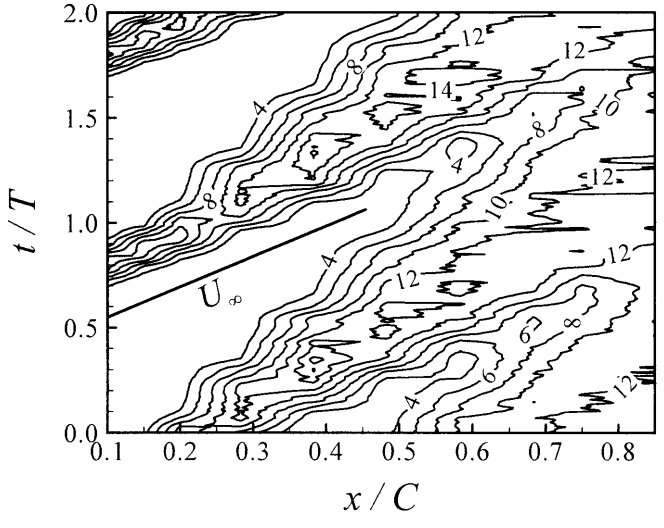

Fig. 5. Contours of the phase-averaged turbulence intensity (%) in the x–t plane near the wall ($y = 0.66$ mm) for the CCW case

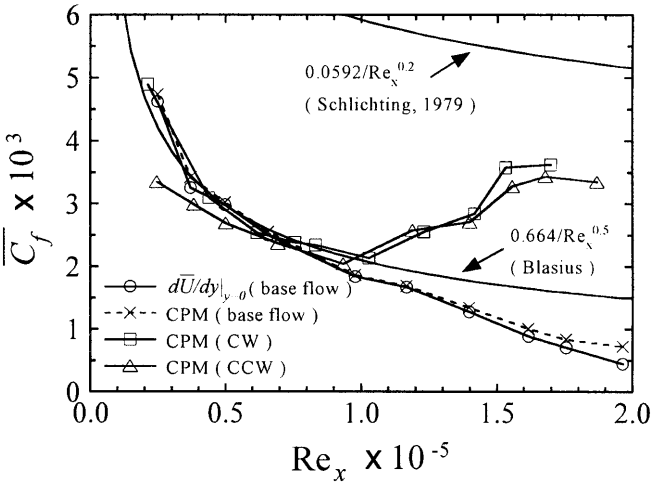

Fig. 6. Time-averaged mean skin-friction coefficients on the airfoil without and with passing wakes

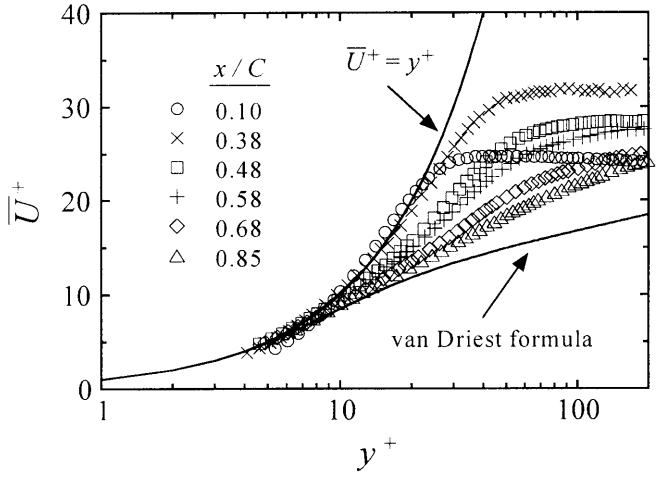

Fig. 7. Time-averaged mean velocity profiles in inner coordinates for the CCW case

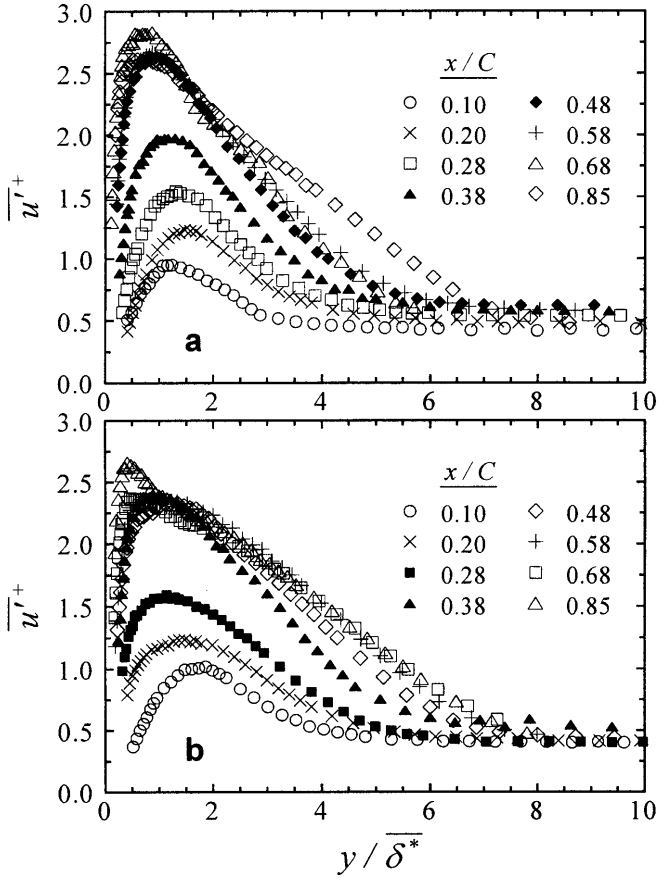

Fig. 8a, b. Time-averaged turbulence fluctuation profiles for **a** the CW case and **b** the CCW case

downstream from transition-onset station, the velocity deviates from the laminar profile more and more, and approaches a typical logarithmic profile of a standard turbulent boundary layer. However, even at the last measuring station ($x/C = 0.85$), the profile still deviates from the logarithmic profile, showing that transition in the time-averaged sense is not completed.

Time-averaged turbulence fluctuations at eight streamwise stations for the CW and CCW cases are presented in Fig. 8a and b, respectively. For both the CW and CCW cases, the peak of the normalized turbulence intensity $\overline{u'}^+$ increases along the downstream station, but even at the last measuring station, the profile of $\overline{u'}^+$ does not access to the fully turbulent value. It is interesting to observe a sudden large increase of the peak at the transition-onset locations, i.e., at $x/C = 0.48$ for the CW case and $x/C = 0.38$ for the CCW case. For the CCW case, before transition onset, high turbulence intensity profile within $0 < y/\overline{\delta^*} < 4$ is slightly wider than that for the CW case. This is because the wake-induced turbulent patch for the CCW case propagates more quickly as explained above. The peaks upstream of transition onset locate away from the wall, e.g., $y \approx 0.15\overline{\delta^*}$ at $x/C = 0.1$ for the CCW case and these approach the wall as flow goes downstream, which is known to a typical behavior of the streamwise turbulence intensity in transition process.

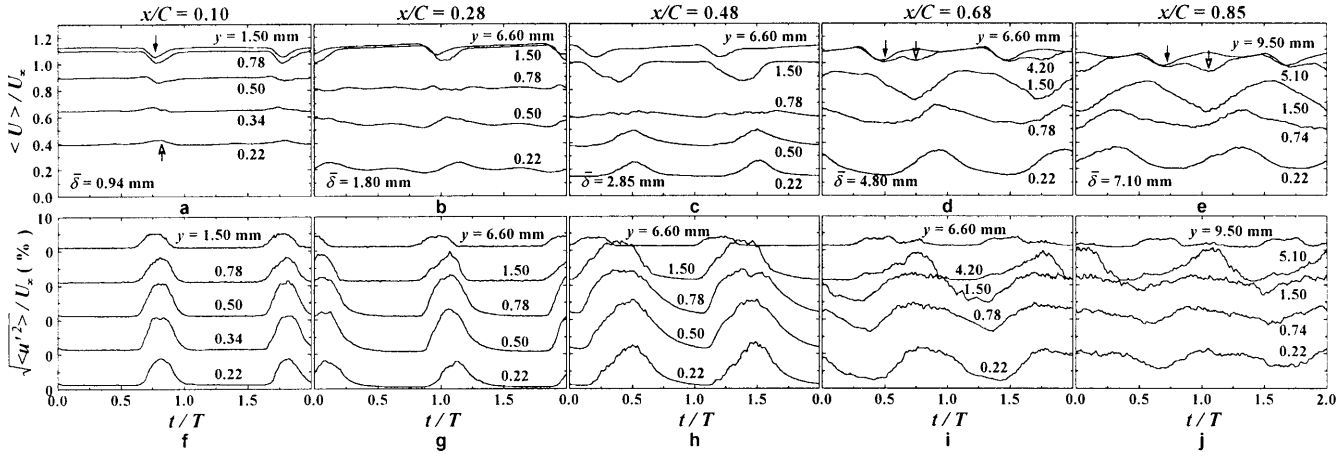

Fig. 9a–j. Temporal variations of the phase-averaged mean velocity and the turbulence intensity at five streamwise locations for the CW case

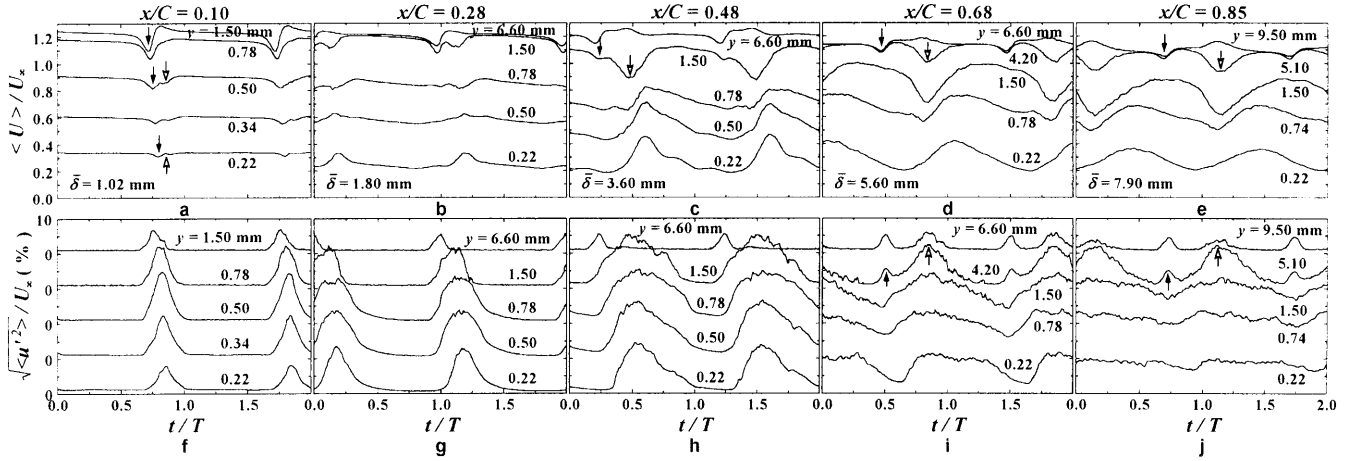

Fig. 10a–j. Temporal variations of the phase-averaged mean velocity and the turbulence intensity at five streamwise locations for the CCW case

3.2.4
Phase-averaged mean velocity and turbulence fluctuation

For the CW case, the normalized phase-averaged mean velocity $\langle U\rangle/U_\infty$ and turbulence intensity $\sqrt{\langle u'^2\rangle}/U_\infty$ are presented at five streamwise locations as a function of normalized phase t/T in Fig. 9a–e and f–j, respectively. At each streamwise location, profiles at five y positions are selectively displayed. To exhibit y position relative to boundary-layer thickness, time-averaged boundary-layer thickness $\bar{\delta}$ is given at each x location. For the CCW case, $\langle U\rangle/U_\infty$ and $\sqrt{\langle u'^2\rangle}/U_\infty$ are also plotted at the same x and y positions as shown in Fig. 10a–e and f–j.

3.2.4.1
Phase-averaged mean velocity and turbulence fluctuation in passing wakes

The defect of the mean velocity and the rise of the turbulence intensity due to the passing wake appear periodically in the free stream. The different characteristics of the passing wake owing to the different wake orientation can be clearly observed in Figs. 9 and 10. The variation of $\langle U\rangle/U_\infty$ at $x/C = 0.1$ and $y = 1.5$ mm (see Figs. 9a, 10a) indicates that for the CW case the width of the wake deficit is larger (the defect is sustained for longer time) but the magnitude of maximum defect is smaller than for the CCW case. For the CW case, the rise of $\sqrt{\langle u'^2\rangle}/U_\infty$ in the wake lasts longer but its peak is smaller than for the CCW case.

As shown in Figs. 9a–e and 10a–e, the phase-averaged mean velocity profiles of the passing wakes are not symmetric with respect to the phase of the maximum defect. For the CW case, there is a slight excess of the mean velocity followed by the velocity defect (the profile at $y = 6.60$ mm in Fig. 9c is most clear). In contrast, for the CCW case, an overshoot of the mean velocity is clearly found just after the wake passes through (see the profile at $y = 1.50$ mm in Fig. 10a). Dong and Cumpsty (1990a, b) and Wu et al. (1999) obtained similar results from an experiment and a numerical simulation, respectively. Especially, Dong and Cumpsty (1990a, b) explained the cause of this result graphically. Figure 11 exhibits four sets of temporal velocity triangles near the leading edge of the airfoil for the CW case. If W_1, W_2, W_3 and W_{ref} are velocities inside the wake in the relative frame, which is moving up at cylinder velocity V_{rod}, the respective inlet resultant velocities in the stationary frame can be drawn as V_1, V_2, V_3 and V_{ref}. Here, V_{ref} is the absolute velocity when no velocity deficit is supposed to exist. If all sets of velocity triangles are exactly drawn, the magnitude of absolute velocities is in the relation of $V_1 > V_3 > V_2$ due to velocity defect in the wake. Because the single hot wire outside the boundary layer detects the velocity signal in serial order of V_{ref}, V_1, V_2, V_3 and V_{ref}, the temporal profile of phase-averaged mean velocity in the wake looks like that at $y = 6.60$ mm in Fig. 9c. The vertical component of V, which results in local increasing of static pressure as discussed in Sect. 3.2.1, becomes maximum at $V = V_2$ as Dong and Cumpsty (1990a, b) also reported. For the CCW case, the magnitude of absolute velocities at the inlet is in the relation of $V_3 > V_1 > V_2$, which is also identified from the profile at $y = 1.50$ mm in Fig. 10a.

An interesting feature is that for the CW case, the mean velocity profile in the wake seems to be absent of any

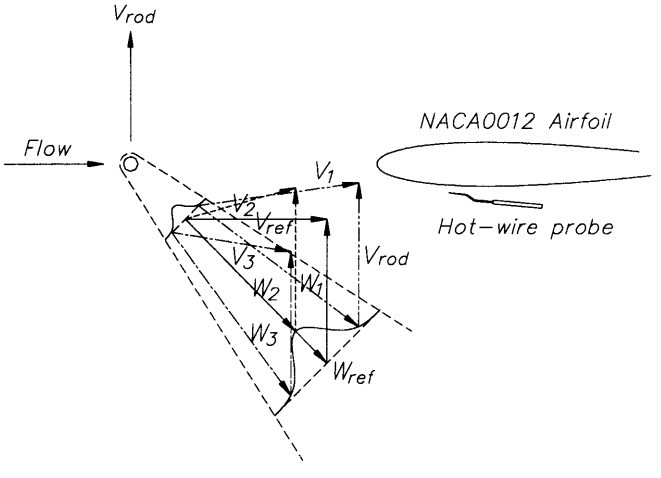

Fig. 11. Example of velocity triangles near the leading edge of the airfoil for the CW case

spreading and decay along the downstream station, whereas the turbulence intensity decays and spreads. For the CCW case, however, both the mean velocity and the turbulence intensity spread and decay in the wake. The absence of wake spreading was also found by Addison and Hodson (1990a, b) in their axial-type-turbine measurements. Liu and Rodi (1991) also observed the same behavior over the wake-induced transitional boundary layer when the cylinder moves downward to the test surface. They supposed that this feature results from the interaction between the wake and the boundary layer or the second passing wakes that are produced by upward cylinder motion at the far end of their rotating wheel. Recently, Funazaki and Aoyama (2000) found that the passing wakes for the reverse rotation case (corresponding to the CCW case) decay more rapidly along the downstream station than for the normal rotation case, which agrees with the present result. From the above previous and present results, it is supposed that the different wake spreading between the CW and CCW cases may be also due to the different streamwise pressure gradients shown in Fig. 2. More detailed studies, however, are required to understand this absence of wake spreading in a wake-affected boundary-layer flow.

3.2.4.2
Phase-averaged turbulence fluctuation inside the boundary layer

As shown in Figs. 9a, f and 10a, f, the turbulence intensity and the mean velocity inside the boundary layer are temporarily disturbed by the passing wake. This explains that the wake-induced turbulent patch passes through the boundary layer and at the almost same time, the flow becomes instantly transitional. After the wake passes over, the mean velocity and the turbulence intensity return to the corresponding initial values of the laminar flow.

A notable feature in Figs. 9f and 10f is that a temporal peak in the turbulence intensity profile becomes maximum at the central part of the boundary layer, i.e., at $y = 0.5$ mm ($y/\bar{\delta} \approx 0.5$) away from the wall for both the CW and CCW cases. Recently, Wu et al. (1999) found that the shape of a wake-induced turbulent spot looks like the arrowhead pointing upstream which was the reverse direction to many previous fundamental studies on natural boundary-layer transition. Zhong et al. (1997) and Kittichaikarn et al. (1999) detected the similar shape of the turbulent patch on the liquid crystal experiments. According to Wu et al. (1999), this phenomenon is observed because the breakdown in wake-induced bypass transition occurs in the outer region of the boundary layer, whereas the breakdown in natural transition takes place near the wall. We found in Figs. 9f–h and 10f–h that when the wake passed over, the peak of the turbulence intensity in the outer region of the boundary layer became higher than that near the wall. This feature seems to be an evidence that breakdown occurs in the outer layer not near the wall.

Before the flow reaches the transition-onset location (Figs. 9f–h and 10f–h), the peaks and widths of the temporal rises in the turbulence intensity profiles increase along the downstream station, indicating the growth of the turbulent patches. However, after transition takes place in the time-averaged sense, these temporal peaks decay along the downstream station as shown in Figs. 9i, j and 10i, j. In particular, at the last measuring x station of the CCW case, the periodic variation of the turbulence intensity mostly disappears near the wall although it still exists in the outer region of the boundary layer. This implies that after merging of the turbulent patches, near-wall turbulence is not sensitive to turbulence characteristics of the traveling wake above the boundary layer, but is mainly affected by instability at the transition onset location and the local streamwise pressure gradients.

3.2.4.3
Phase-averaged mean velocity inside the boundary layer

The phase-averaged mean velocity inside the boundary layer is perturbed by the velocity defect in the passing wake and the wake-induced turbulent patch. At Figs. 9 and 10, solid arrows indicate representative $\langle U \rangle$ or $\sqrt{\langle u'^2 \rangle}$ which are temporarily changed by the external wake deficits. On the other hand, open ones present representative $\langle U \rangle$ or $\sqrt{\langle u'^2 \rangle}$ perturbed instantly by wake-induced turbulent patch inside the boundary layer.

Figures 9a and 10a ($x/C = 0.1$) show that the mean velocity profiles in the boundary layer have a periodic dip due to the influence of the wake deficit. When approaching the wall, the magnitude of this dip becomes smaller and its phase is gradually delayed because of the high viscous diffusion in near-wall flows. For the CCW case, this velocity dip is still alive even at the most inner y location ($y = 0.22$ mm), while, for the CW case, the mean velocity peak appears at the same y location instead of the velocity dip. This means that due to the turbulent patch, the boundary layer becomes temporarily transitional, having larger velocity gradient near the wall but a lower value of the mean velocity in the outer region than the laminar boundary layer. For the CCW case, the small peak also appears following the velocity dip at $y = 0.22$ mm.

It is interesting to note from Fig. 10a that for the CCW case, the mean velocity profile at outer boundary layer ($y = 0.5$ mm) has two small dips within one passing period. The dual dips at the outer region of boundary layer are more clearly found downstream of transition-onset location (Fig. 10d, e). These two dips correspond to the two peaks in the turbulence intensity profile at the same y location and at the almost same phase as shown in Fig. 10i, j. The early dip of the mean velocity is from wake deficit and its late dip results from temporal thickening of boundary layer due to the turbulent patch. For the CW case, two dips in mean velocity profiles also appear clearly at outer parts of the boundary layer as shown in Fig. 9d, e, whereas the corresponding two peaks in turbulence intensity profiles are not observed in Fig. 9i, j. Liu and Rodi (1991) and Wu et al. (1999) also observed similar mean velocity dual dips in the outer parts of boundary layers. Liu and Rodi (1991) supposed two possibilities as the reason of these two dips. The first was from secondary wake generated inevitably in their rotating wheel and the second was from the wake-induced turbulent patches. Wu et al. (1999) demonstrated that the latter was the major cause of two velocity dips, which was also confirmed

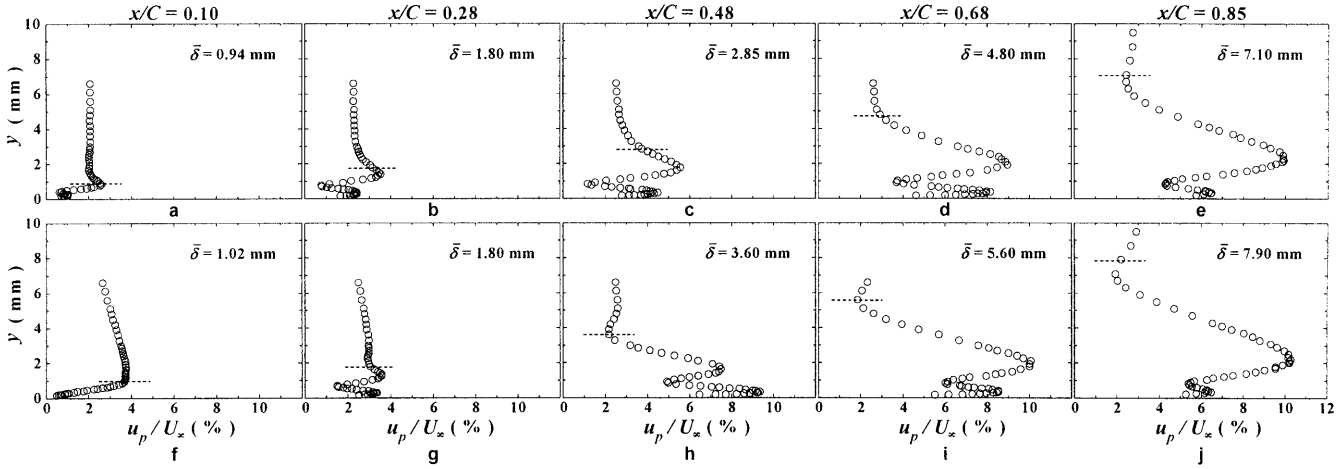

Fig. 12a–j. Distributions of rms values of periodic fluctuating velocity at five streamwise locations for **a–e** the CW case and **f–j** the CCW case

in the present experiment. Downstream of $x/C = 0.28$ (Figs. 9b–e and 10b–e), the mean velocity dip due to the wake deficit is not found near the wall, while that due to the wake-induced turbulent patch is observed in most parts of the boundary layer.

The behavior for the periodic velocity component $\tilde{u}$ in the boundary layer can be seen explicitly in Fig. 12, which shows y-profiles of the rms value (u_p) of $\tilde{u}$ for the CW (Fig. 12a–e) and CCW (Fig. 12f–j) at the same x locations as in Figs. 9 and 10. The horizontal dashed line in these figures indicates the time-averaged edge of the boundary layer. For the CW case, the periodic velocity fluctuation at the free stream remains almost constant along the downstream station because the wake seems to be in the absence of any decay as discussed in Sect. 3.2.4.1. For both the CW and CCW cases, the profile of u_p has two distinguished peaks in the boundary layer at most x locations. The peak of u_p in the outer layer is from the periodic decrease/recovery of the mean velocity due to the passing of the turbulent patch. In contrast, the near-wall peak results from the periodic increase/recovery of the mean velocity due to the patch. Therefore, owing to the switching-over of this different behavior, a local minimum of u_p appears between the y positions of the two peaks. The peak of u_p in the outer layer increases continuously as the flow goes downstream. In contrast, the near-wall peak attains a maximum at $x/C = 0.68$ for the CW case and at $x/C = 0.48$ for the CCW case, and then decreases along the downstream station.

3.2.5
Phase-averaged wall skin friction

Figure 13 shows the x–t plane distributions of the normalized phase-averaged friction velocity $\langle u_\tau \rangle / U_\infty$ (line contour) on the airfoil surface and phase-averaged turbulence intensity $\sqrt{\langle u'^2 \rangle}/U_\infty$ (color contour) at $y = 0.34$ mm for the CCW case. The location $y = 0.34$ mm is where the near-wall peak of u_p appears as shown in Figs. 12f–j for the CCW case. The profile of $\langle u_\tau \rangle$ is very similar to that of the near-wall $\sqrt{\langle u'^2 \rangle}$ except that the former lags entirely behind the latter, showing that the characteristic of wall skin friction is noticeably concerned with that of near-wall turbulence, i.e., the wake-induced turbulent patch. Upstream of the transition-onset location, $\langle u_\tau \rangle$ rises right after the high turbulence intensity passes through, illustrating again that the boundary layer becomes temporarily transitional due to the passing of the turbulent patch. The streamwise expansion of high friction velocity regions along the downstream station is caused by the growth of turbulent patch. The phase-lag between the fairly large friction velocity and the corresponding high turbulence intensity increases gradually as flow goes downstream. For the CCW case, the $\langle u_\tau \rangle / U_\infty$ larger than 4.5% appears first at about $x/C = 0.4$, while for the CW case (not shown here), it is found at about $x/C = 0.55$. This confirms again that the onset of transition occurs further

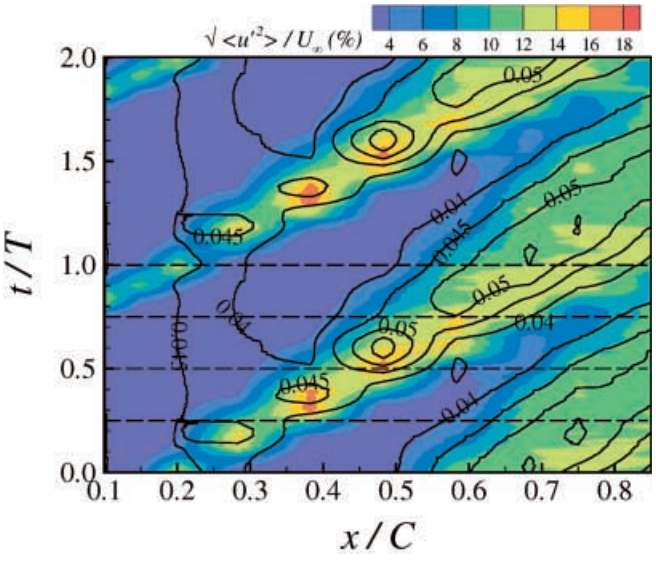

Fig. 13. Contours of the normalized phase-averaged friction velocity $\langle u_\tau \rangle / U_\infty$ (line contour) and turbulence intensity $\sqrt{\langle u'^2 \rangle}/U_\infty$ (%, color contour) at $y = 0.34$ mm in the x–t plane for the CCW case

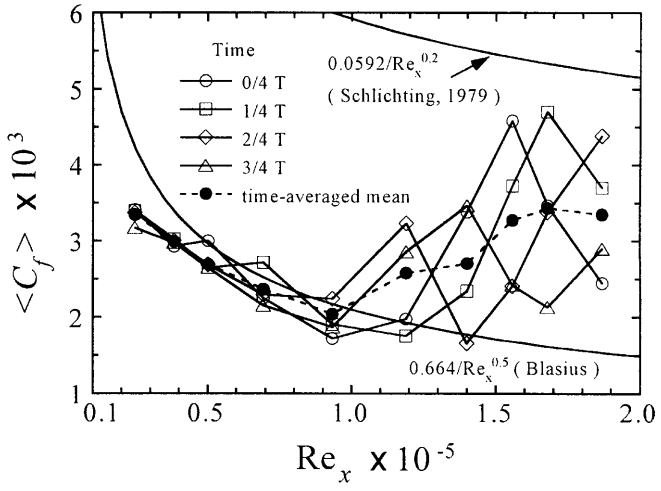

Fig. 14. Streamwise profiles of the phase-averaged skin-friction coefficient at four different phases during one passing period for the CCW case

upstream for the CCW case than for the CW case. Propagation velocities for the center of the friction velocity contours are about $0.72U_\infty$ and $0.63U_\infty$ for the CW and CCW cases, respectively. These are less than the corresponding propagation rates for the center of the turbulent patch at $y = 0.34$ mm, i.e., $0.78 \sim 0.86U_\infty$ for the CW case and $0.72 \sim 0.78U_\infty$ for the CCW case.

Figure 14 shows streamwise variations of the phase-averaged skin-friction coefficient for the CCW case at four phases, i.e., 0, 1/4T, 2/4T, and 3/4T, which are indicated as the horizontal dashed lines in Fig. 13. A local small rise of $\langle C_f \rangle$ in the laminar region is caused by the passing of turbulent patch. Its large rise downstream of the transition onset location results from the growth and merging of the patches. Downstream of transition onset, an interesting feature in the $\langle C_f \rangle$ variation can be found. In the profile at the 2/4T phase line, a local minimum at about $Re_x = 1.4 \times 10^5$ following a local peak at about $Re_x = 1.2 \times 10^5$ is somewhat lower than the Blasius solution, implying that the boundary-layer flow recovers to the initial laminar state after the passing of the turbulent patch. In contrast, in the profile at the 3/4T phase line, a local minimum at about $Re_x = 1.7 \times 10^5$ following a local peak at about $Re_x = 1.4 \times 10^5$ does not recover to the laminar value and is sustained to the transitional value. Therefore, it is supposed that the self-sustained turbulence evolves from at least $Re_x = 1.7 \times 10^5$ due to the merging of the turbulent patches. A similar behavior of $\langle C_f \rangle$ can be seen in the DNS result of Wu et al. (1999).

Figure 15a,b presents the streamwise variation of rms periodic skin-friction fluctuation coefficient γ_{C_f} defined as

$$\gamma_{C_f} = \left\{ \overline{\left(\langle C_f \rangle - \overline{C_f} \right)^2} \right\}^{1/2} \Big/ \overline{C_f} \qquad (3)$$

for the CW and CCW cases. As presented and discussed in Wu et al. (1999), γ_{C_f} is a good indicator for the transitional state of the boundary-layer flow. As also included in Fig. 15, other possible indicators for the transitional state are the near-wall peak ($u_{p,peak}$) of u_p and the difference

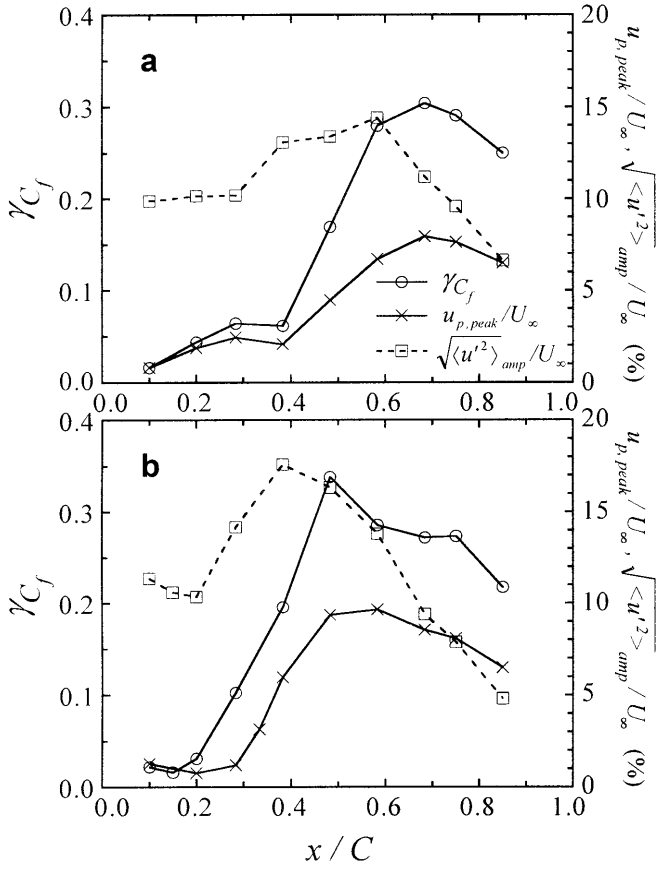

Fig. 15a, b. Streamwise profiles of γ_{C_f}, $u_{p,peak}/U_\infty$ (%) and $\sqrt{\langle u'^2 \rangle}_{amp}/U_\infty$ (%) at $y = 0.34$ mm for **a** the CW case and **b** the CCW case

$\left(\sqrt{\langle u'^2 \rangle}_{amp} \right)$ between maximum and minimum of $\sqrt{\langle u'^2 \rangle}$ at $y = 0.34$ mm obtained from of Figs. 9f–j and 10f–j. Near the leading edge of the airfoil, γ_{C_f} and $u_{p,peak}$ have small values close to zero, whereas $\sqrt{\langle u'^2 \rangle}_{amp}$ maintains a relatively large value. γ_{C_f} has maximum value of about 0.30 at $x/C = 0.68$ for the CW case and about 0.34 at $x/C = 0.48$ for the CCW, meaning that at these x locations, the corresponding boundary-layer flow is in the most transitional state. Wu et al. (1999) also obtained a similar value of 0.33 as the global maximum of γ_{C_f}. This may be because the Strouhal number of 0.57, which is based on the closest distance between the cylinder and airfoil ($St_b = fb/U_\infty$) in the present experiment, is very similar to the corresponding value of 0.6 in their numerical simulation. An interesting feature in Fig. 15 is that the x location of maximum $u_{p,peak}$ is coincident with that of maximum γ_{C_f}, indicating that the phase-averaged mean velocity near the wall oscillates with the largest amplitude when the boundary-layer flow becomes most transitional, which is also reported by Wu et al. (1999). However, the maximum $\sqrt{\langle u'^2 \rangle}_{amp}$ appears slightly further upstream of the x location of maximum γ_{C_f} and $u_{p,peak}$. This means that the near-wall turbulence responds to the passing wake more quickly than the wall skin friction and the near-wall mean velocity. Downstream of the location of the maximum value, γ_{C_f} decreases together with $u_{p,peak}$ and $\sqrt{\langle u'^2 \rangle}_{amp}$. If the airfoil were sufficiently long, all of γ_{C_f}, $u_{p,peak}$ and

$\sqrt{\langle u'^2 \rangle}_{amp}$ would approach zero after the transition is completed in the time-averaged sense.

4 Conclusions

Wake-induced transition in boundary-layer flows developing on a NACA 0012 airfoil was experimentally investigated. The wakes were periodically generated by rotating circular cylinders clockwise and counterclockwise around the airfoil. The phase-averaged technique for the streamwise velocity was employed to investigate the phenomena of wake-induced transition in detail, and particularly, the phase-averaged wall shear stress was reasonably estimated using the computational Preston tube method. Several conclusions are listed below:

(1) The streamwise distribution of time-averaged pressure on the airfoil was significantly changed due to the passing wakes. The pressure profile on the airfoil changed significantly depending on the orientation of the passing wakes. In the case of CW rotation, the whole pressure gradient was reduced, whereas in the case of CCW rotation, it was increased. This alteration of the pressure profile greatly affected the transition process of the boundary layer.

(2) The wake-induced turbulent patches inside the laminar boundary layer for the CCW case grew more quickly and merged with each other further upstream than those for the CW case. In other words, transition onset in the time-averaged sense occurred further upstream for the CCW case, which could be also confirmed in the profiles of time-averaged wall skin friction. This is because the initial patch generated near the leading edge had higher turbulence intensity and the local streamwise adverse pressure gradient became larger for the CCW case. In addition, because of the same reasons, the separation between the turbulent patch and the wake occurred for the CCW case.

(3) Before the onset of transition, the peak of the phase-averaged turbulence intensity was found to attain maximum in the outer part of the boundary layer not near the wall. This was evidence that breakdown in wake-induced transition occurred in the outer region of the boundary layer as recently proposed by Wu et al. (1999).

(4) After the turbulent patches started merging with each other, near-wall turbulence was not sensitive to the turbulence property of traveling wakes over the boundary layer. They were mainly affected by instability at the transition-onset location and streamwise pressure distribution downstream of the transition-onset location.

(5) The phase-averaged streamwise velocity had two dips in the outer boundary layer for each wake-passing period. One was caused by the wake deficit and the other caused by temporal thickening of the boundary layer due to the passing of the wake-induced turbulent patch.

(6) The x location of maximum $u_{p,peak}$ was coincident with that of maximum γ_{C_f}, whereas that of maximum $\sqrt{\langle u'^2 \rangle}_{amp}$ appeared slightly further upstream. This implies that near-wall turbulence responds to the passing wake more quickly than the wall skin friction and the near-wall mean velocity.

References

Addison JS; Hodson HP (1990a) Unsteady transition in an axial flow turbine. Part 1. Measurements on the turbine rotor. ASME J Turbomachinery 112: 206–214

Addison JS; Hodson HP (1990b) Unsteady transition in an axial flow turbine. Part 2. Cascade measurements and modeling. ASME J Turbomachinery 112: 215–221

Chakka P; Schobeiri MT (1999) Modeling unsteady boundary layer transition on a curved plate under periodic unsteady conditions: aerodynamics and heat transfer investigations. ASME J Turbomachinery 121: 88–97

Cho N-H; Liu X; Rodi W; Schönung B (1993) Calculation of wake-induced unsteady flow in a turbine cascade. ASME J Turbomachinery 115: 675–686

Dong Y; Cumpsty NA (1990a) Compressor blade boundary layers. 1. Test facility and measurements with no incident wakes. ASME J Turbomachinery 112: 222–230

Dong Y; Cumpsty NA (1990b) Compressor blade boundary layers. 2. Measurements with incident wakes. ASME J Turbomachinery 112: 231–240

Fan S; Lakshminarayana B (1996) Computation and simulation of wake-generated unsteady pressure and boundary layers in cascades. 1. Description of the approach and validation. ASME J Turbomachinery 118: 96–108

Funazaki K; Aoyama Y (2000) Studies on turbulence structure of boundary layers disturbed by moving wakes. ASME Paper 2000-GT-0272

Funazaki K; Koyabu E (1999) Effects of periodic wake passing upon flat-plate boundary layers experiencing favorable and adverse pressure gradients. ASME J Turbomachinery 121: 333–340

Gostelow JP; Melwani N; Walker GJ (1996) Effects of streamwise pressure gradient on turbulent spot development. ASME J Turbomachinery 118: 737–743

Halstead DE; Wisler DC; Okiishi TH; Walker GJ; Hodson HP; Shin H (1997) Boundary layer development in axial compressors and turbines. 1. Composite picture. ASME J Turbomachinery 119: 114–127

Hodson HP (1985) Measurements of wake-generated unsteadiness in the rotor passages of axial flow turbines. ASME J Eng Gas Turbines Power 107: 467–476

Jeon WP; Kang SH (1995) Measurement of transitional boundary layer on a flat plate using a computational Preston tube method. Exp Fluids 20: 29–37

Jeon WP; Shin SH; Kang SH (2000) Prediction of wall shear stress in transitional boundary layers using near-wall mean velocity profiles. Korean Soc Mech Eng Int J 14: 1297–1310

Kim K; Crawford ME (2000) Prediction of transitional heat transfer characteristics of wake-affected boundary layers. ASME J Turbomachinery 122: 78–87

Kittichaikarn C; Ireland PT; Zhong S; Hodson HP (1999) An investigation on the onset of wake-induced transition and turbulent spot production rate using thermochromic liquid crystals. ASME Paper 99-GT-126

Lee HK; Kang SH (2000) Flow characteristics of transitional boundary layers on an airfoil in wakes. ASME J Fluid Eng 122: 522–532

Liu X; Rodi W (1991) Experiments on transitional boundary layers with wake-induced unsteadiness. J Fluid Mech 231: 229–256

Mayle RE (1991) The role of laminar-turbulent transition in gas turbine engines. ASME J Turbomachinery 113: 509–537

Mayle RE; Dullenkopf K (1991) More on the turbulent-strip theory for wake-induced transition. ASME J Turbomachinery 113: 428–432

Nitsche W; Thunker R; Haberland C (1983) A computational Preston tube method. Turbulent Shear Flows 4: 261–276
Orth U (1993) Unsteady boundary layer transition in flow periodically disturbed by wakes. ASME J Turbomachinery 115: 707–713
Pfeil H; Herbst R; Schröder T (1983) Investigation of the laminar-turbulent transition of boundary layers disturbed by wakes. ASME J Eng Power 105: 130–137
Schlichting H (1979) Boundary layer theory. McGraw-Hill, New York
Schulte V; Hodson HP (1998) Unsteady wake-induced boundary layer transition in high lift LP turbines. ASME J Turbomachinery 120: 28–35
Walker GJ (1993) The role of laminar-turbulent transition in gas turbine engines: a discussion. ASME J Turbomachinery 115: 207–217
Walker GJ; Hughes JD; Solomon WJ (1999) Periodic transition on an axial compressor stator: incidence and clocking effects. 1. Experimental data. ASME J Turbomachinery 121: 398–407
Wu X; Jacobs RG; Hunt JCR; Durbin PA (1999) Simulation of boundary layer transition induced by periodically passing wakes. J Fluid Mech 398: 109–153
Zhong S; Kittichaikarn C; Hodson HP; Ireland PT (1997) Study of turbulent spots with temperature-sensitive liquid crystals. In: Proceedings of the of 2nd International Symposium on Turbulence, heat and mass transfer, Delft, The Netherlands